Counts and Colors of Faint Galaxies in the U and R Bands[1]

David W. Hogg,[2] Michael A. Pahre,[3] James K. McCarthy,[3] Judith G. Cohen,[3]
Roger Blandford,[2] Ian Smail,[4] & B. T. Soifer[3]

ABSTRACT

Ground-based counts and colors of faint galaxies in the U and R bands in one field at high Galactic latitude are presented. Integrated over flux, a total of 1.2×10^5 sources per square degree are found to $U = 25.5$ mag and 6.3×10^5 sources per square degree to $R = 27$ mag, with $d \log N/dm \sim 0.5$ in the U band and $d \log N/dm \sim 0.3$ in the R band. Consistent with these number-magnitude curves, sources become bluer with increasing magnitude to median $U - R = 0.6$ mag at $24 < U < 25$ mag and $U - R = 1.2$ mag at $25 < R < 26$ mag. Because the Lyman break redshifts into the U band at $z \approx 3$, at least 1.2×10^5 sources per square degree must be at redshifts $z < 3$. Measurable U-band fluxes of 73 percent of the 6.3×10^5 sources per square degree suggest that the majority of these also lie at $z < 3$. These results require an enormous space density of objects in any cosmological model.

Subject headings: Galaxies: fundamental parameters — Galaxies: photometry — Cosmology: observations — Ultraviolet: galaxies

1. Introduction

The number of faint galaxies as a function of apparent magnitude is one of the fundamental observational constraints on cosmology and galaxy evolution. The first such measurements made with CCDs and automated source detection algorithms (Hall &

MacKay 1984; Tyson 1988), showed signs of an excess over predictions based on naive extrapolations of local galaxy properties. Recent ground-based galaxy counts to $B = 27.5$ (Metcalfe et al 1995), $V = 27$, $R = 27$ $I = 25.5$ (Smail et al 1995), and $K = 24$ mag (Djorgovski et al 1995) all reach integrated number densities around 6×10^5 per square degree and show numbers increasing by a factor of ~ 2 per magnitude, or $d \log N/dm \sim 0.3$ in the red and near-infrared. Given local luminosity function determinations (e.g., Loveday et al 1992), these high numbers require either strong source evolution or extreme world models; it is certainly possible that a number of effects contribute. Furthermore, the variation of the slope $d \log N/dm$ with observed waveband, showing increased slope ~ 0.5 in the B-band and ~ 0.6 in the U-band and corresponding blueing of the objects with apparent magnitude (see Koo & Kron 1992, for a review) is an important clue to the physical processes generating the radiation in these objects.

The Hubble Space Telescope (HST) has proven very effective in the field of faint galaxy counts, benefitting from reduced sky brightness and the small angular sizes of faint galaxies (Smail et al 1995), which are only marginally resolved even with HST/WFC's 0.1 arcsec resolution. In a 3×10^4 s HST exposure, Cowie et al (1995) count objects in the field to $I = 26$, finding $\approx 8 \times 10^5$ per square degree. More recently, in the Hubble Deep Field (Williams et al 1996), 1.5×10^5 s HST exposures were taken in each of four filters in a single field; counts by Williams et al (1996) find roughly 10^6 objects per square degree to $(F606W)_{AB} \approx 30$ mag.

Galaxy counts in the U-band have not been pushed to numbers nearly as high as those in other optical bands. The subject is interesting because what U-counts do exist show the number counts to rise very rapidly, by a factor of 3 or 4 per magnitude or $d \log N/dm \sim 0.5$ or 0.6 (Koo 1986; Songaila et al 1990; Jones et al 1991); i.e., U-band counts are much steeper than counts at longer wavelengths. We present the deepest published galaxy counts in the U-band, reaching $U \approx 25.5$ mag, in an image taken under conditions of good seeing with the Hale Telescope, along with galaxy counts in the R-band, in a deep image taken with the W. M. Keck Telescope. We also present $U - R$ colors to look for the color trend implied by the difference in count slopes. In terms of point-source sensitivity, the U-band image presented here will be surpassed by ultra-deep HST observations (such as those in the Hubble Deep Field) but this image has very good surface-brightness sensitivity and a much wider field of view.

At $z > 3$, the observed U band is at emitted wavelengths shortward of the Lyman limit, which is expected to be optically thick to absorption by neutral hydrogen in the intergalactic medium. This would be observed as anomalously low U-band flux, or anomalously red $(U - B)$ colors for any population of $z > 3$ objects. Guhathakurta et al (1990) used the lack

of such objects to demonstrate that to $R = 26$ mag, faint galaxy counts are not dominated by objects at $z > 3$. Steidel et al (1995) have counted and, recently, spectroscopically confirmed (Steidel et al 1996) a population of objects identified for anomalously red $(U - G)$ colors and find that there are ~ 1500 objects in redshift range $3 < z < 3.4$ per square degree to $R \approx 25$ mag.

2.   Field selection and observations

The field, RA $00^h\,53^m\,23\overset{s}{.}20$, Dec $+12° 33' 57\overset{''}{.}5$ (J2000), was chosen for the purposes of deep K-band imaging (Djorgovski et al 1995) and a faint object redshift survey (Cohen et al 1996a) from among existing deep Medium Deep Survey (Griffiths et al 1994) HST images which are taken in parallel mode in fields selected for low extinction and high Galactic latitude. The particular MDS field was chosen for its long HST exposure time and high Galactic latitude to minimize stellar contamination. Additional ground-based photometry on this field will be reported by Pahre et al (1996) and the detailed results of the redshift survey will be reported by Cohen et al (1996c).

The U-band data were taken in 1995 September with the COSMIC instrument (Dressler 1993) at the prime focus of the 5 m Hale Telescope. Palomar CCD13, a Tektronix 2048×2048 array of 24 μm pixels (TK2048), was used in place of the standard COSMIC TK2048 CCD owing to high near-UV sensitivity of CCD13. Individual 600 s exposures were taken on a 5×5 grid with roughly 10 arcsec spacing. The seeing is 1.1 arcsec in the final stacked image. Patchy cloud cover necessitated independent photometric calibration (see below).

The R-band data were taken during periods of fair seeing (0.8 arcsec in the final stacked image) on spectroscopic runs in 1995 July and August with the Low Resolution Imaging Spectrograph (LRIS) (Oke et al 1995) on the 10-m Keck Telescope. Individual 600 s exposures were taken at dithers of several arcseconds with respect to one another. A temporary problem with the telescope caused the individual R-band exposures to be contaminated with transient, non-repeating streaks of scattered light, from bright stars outside the field reflecting from telescope structures. This limits the quality of the R image flatfield and background estimation, and reduces the completeness and quality of the photometry at very faint levels. In removing the streaks, small gradients on scales of ~ 20 arcsec were eliminated (taking with them any hypothetical population of large, low-surface-brightness galaxies; of course the detection algorithm is not optimized for such objects anyway). Again patchy cloud cover necessitated independent photometric calibration.

For both the U-band and R-band data, before stacking, individual images were shifted and geometrically remapped to a Cartesian plane according to a distortion map determined from the dithered images themselves. The remapped, shifted images were stacked with the *IRAF/imcombine* task, making use of sigma-clipping to remove cosmic rays. Matched 1×1 arcmin^2 sections of the stacked Hale U and Keck R-band images are shown in Figs. 1 and 2, and observational details are summarized in Table 1.

The U and R-band images were calibrated with U and R_{C}-band CCD images taken under photometric conditions with CCD13 on the Palomar Sixty-Inch Telescope (P60). The details of the P60 data reduction are presented in Pahre et al (1996). Calibration shows that the filter and CCD used on the Hale Telescope make a non-standard U bandpass, which we denote "U_{13}". We find $U = U_{13} + 0.06\,(U_{13} - R)$. In the following we use U_{13} but the magnitudes can be corrected to pseudo-U-band by adding 0.08 mag, correct for a typical faint object, which has $(U_{13} - R) = 1.3$ mag. This correction is on the same order as the estimated uncertainty in the calibration, between 0.05 and 0.1 mag.

3.   Analysis

3.1.   Object detection

Objects are detected in both the U and R-band images with the image analysis package *SExtractor* (Bertin & Arnouts 1996). The algorithm is: (1) fit a smooth surface to the background; (2) convolve the image with a Gaussian filter with FWHM matched to the PSF; and (3) find objects above the threshold which corresponds to a point source with $U_{13} = 25.63$ mag or $R = 28.49$ mag. Often detected objects have multiple peaks; a peak is split off into its own object only if its part of the object contains > 10 percent of the total flux. We did not use the package for star/galaxy separation or any "cleaning" of spurious detections. Stars only make up a small fraction of the faint sources at high Galactic latitude (Smail et al 1995) and cleaning spurious objects is handled by our noise object and completeness corrections described below.

3.2.   Photometry

In order to match the seeing of our images (1.1 arcsec FWHM in the U-band and 0.8 arcsec in the R-band), aperture photometry is performed in 1.5 arcsec diameter apertures, which is between 1.3 and 2 times the seeing FWHM. To these aperture magnitudes aperture corrections are added to attempt, in a statistical way, to account for
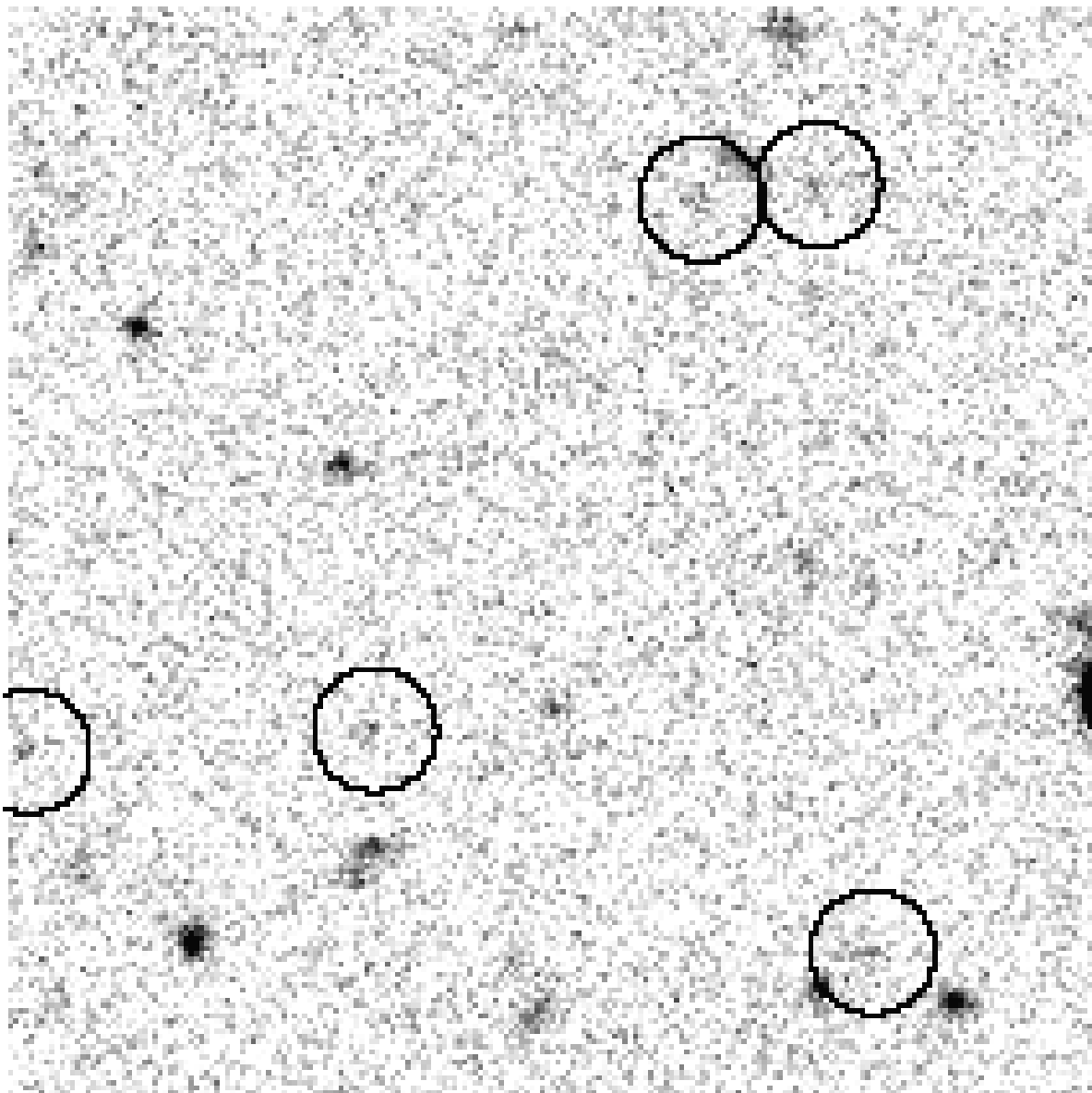
Fig. 1.— A 1×1 arcmin^2 section of the final, stacked U-band image. Sources with $25.0 < U_{13} < 25.5$ mag are circled.
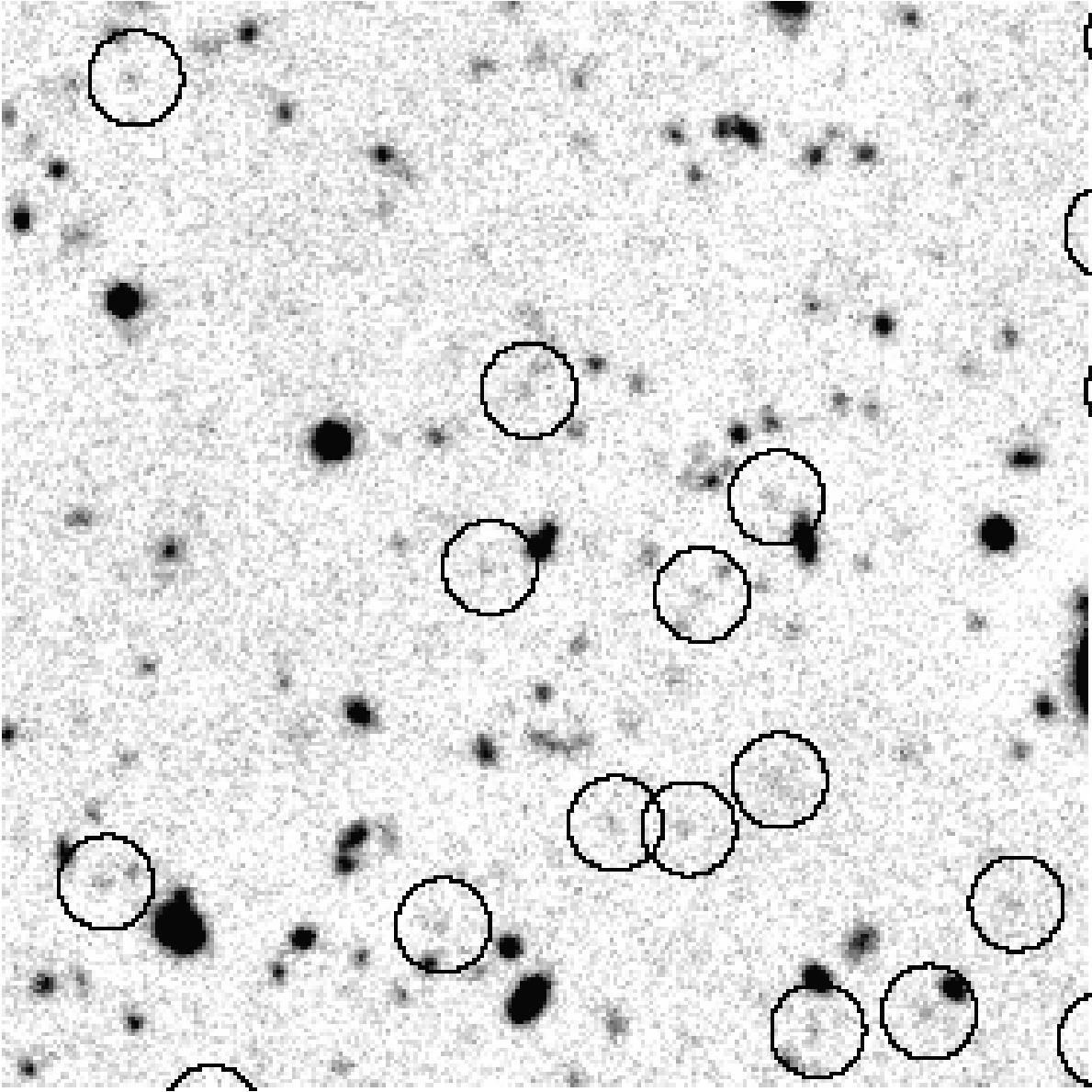
Fig. 2.— A 1×1 arcmin^2 section of the final, stacked R-band image, matched to Fig. 1. Sources with $26.5 < R < 27.0$ mag are circled.

object flux coming from outside the aperture. The faintest objects are consistent with having stellar profiles, in these images and even in R-band images with superior seeing (Smail et al 1995), so we added the stellar correction, -0.60 mag in the U-band image and -0.25 mag in the R-band. For all objects we also measure a 1σ isophotal magnitude to which is added an aperture correction varying linearly from 0 to -0.60 over the range $23.5 < U_{13} < 25.5$ mag and from 0 to -0.25 over $24.5 < R < 26.0$ mag. Every object is assigned the brighter of the two corrected magnitudes.

The reddening in this field is $A_V = 0.13$ mag (Burstein & Heiles 1982) so we corrected the U-band fluxes by 0.20 mag and R-band by 0.11 mag.

3.3.   Removal of noise objects

The transforming, shifting and stacking of the images introduces pixel-to-pixel correlations in the noise, making it difficult to estimate analytically the contamination of the counts by spurious detections of peaks in the noise. Spurious detections of this type are corrected-for in a statistical way, by subtracting "noise counts" from the positive counts. Noise counts are estimated by running the detection and photometry algorithms on the images but searching for negative rather than positive objects. The raw negative counts are subtracted from the raw positive counts before applying completeness corrections (see below) and all Poisson error bars include the uncertainty added by this procedure. In the U-band image, noise objects account for 10 and 29 percent of the objects in the two faintest half-magnitude bins and in the R-band image, only 0.6 and 8 percent in the two faintest half-magnitude bins.

Spurious objects are sometimes produced by cosmic ray hits. However, so many individual exposures (47 in U_{13}, 14 in R) were stacked with the sigma-clipping algorithm that no significant-flux cosmic-ray events could plausibly remain.

3.4.   Completeness correction

The counts are corrected for completeness in a manner similar to that of Smail et al (1995). Detected objects are cut out of the final U and R-band images, dimmed by a factor of 10, and added back into randomly selected subfields. The detection algorithm is run and the catalogs of objects in the subfields are compared before and after adding the additional object. By this procedure we generate a "completeness matrix" P_{ij} which stores the probability that an added object of true magnitude m_i is in fact detected with

magnitude m_j. Because some objects are not recovered at all and because others are blended into existing brighter objects, etc., the sum over j of P_{ij} will not in general be unity. The completeness information is a matrix because the statistical incompleteness in each magnitude bin depends on the true functional form of the number-magnitude plot; however, under the assumption that the galaxy count slopes do not change dramatically over the magnitude range of interest, this matrix converts naturally into a fractional completeness as a function of magnitude.

To construct P_{ij} in practice, bright objects were cut out of the images, dimmed by a factor of 10, replaced at random locations, and then searched-for and photometered by the detection algorithm. In the U-band image, 10^5 random replacements were performed, and in the R-band image, 6×10^4, with the number increasing with magnitude in proportion to the counts. Each element of the matrix also has an associated uncertainty from Poisson statistics. The detection fraction f_j in each bin was generated by assuming that the U counts follow a power law $d \log N/dm \approx 0.47$ and that the R counts follow power law $d \log N/dm \approx 0.33$. Our noise-object-subtracted, completeness-corrected U and R-band object counts are shown in Figs. 3 and 4, along with the completeness-corrected counts of other authors. Note that because this completeness correction corrects not just for missing numbers but also for photometry errors, and because the counts increase with magnitude, it is possible for the completeness correction near (but not at) the detection threshold to be negative, as is seen for at least one point in Fig. 3.

Faint objects get smaller in angular size with increasing magnitude (Smail et al 1995; Im et al 1995), and since more compact objects are easier to detect at the same flux level, the detected fractions calculated by this technique would, in better data, be lower limits. A better procedure would involve changing the angular sizes of the objects as well as dimming them before replacing them. However, the seeing in our images is not good enough for the changing sizes to be a significant effect at faint levels.

3.5. Color measurement

Magnitudes through 1.5 arcsec diameter apertures, measured with the NOAO *apphot* package, were subtracted to make $(U - R)$ colors for the entire R-selected sample to $R = 27$ and that part of the U-selected sample which overlaps the R-band image to $U = 25$. Median colors as a function of magnitude and color histograms for several U-selected and R-selected subsamples are shown in Figure 5. To $R = 27$ mag, 73 percent of the sources in the R-band image are detected with a confidence of $1\,\sigma$ or better in the U-band image. The median measured color in the faintest U-band magnitude bin is $U - R = 0.6$ mag. In the faintest
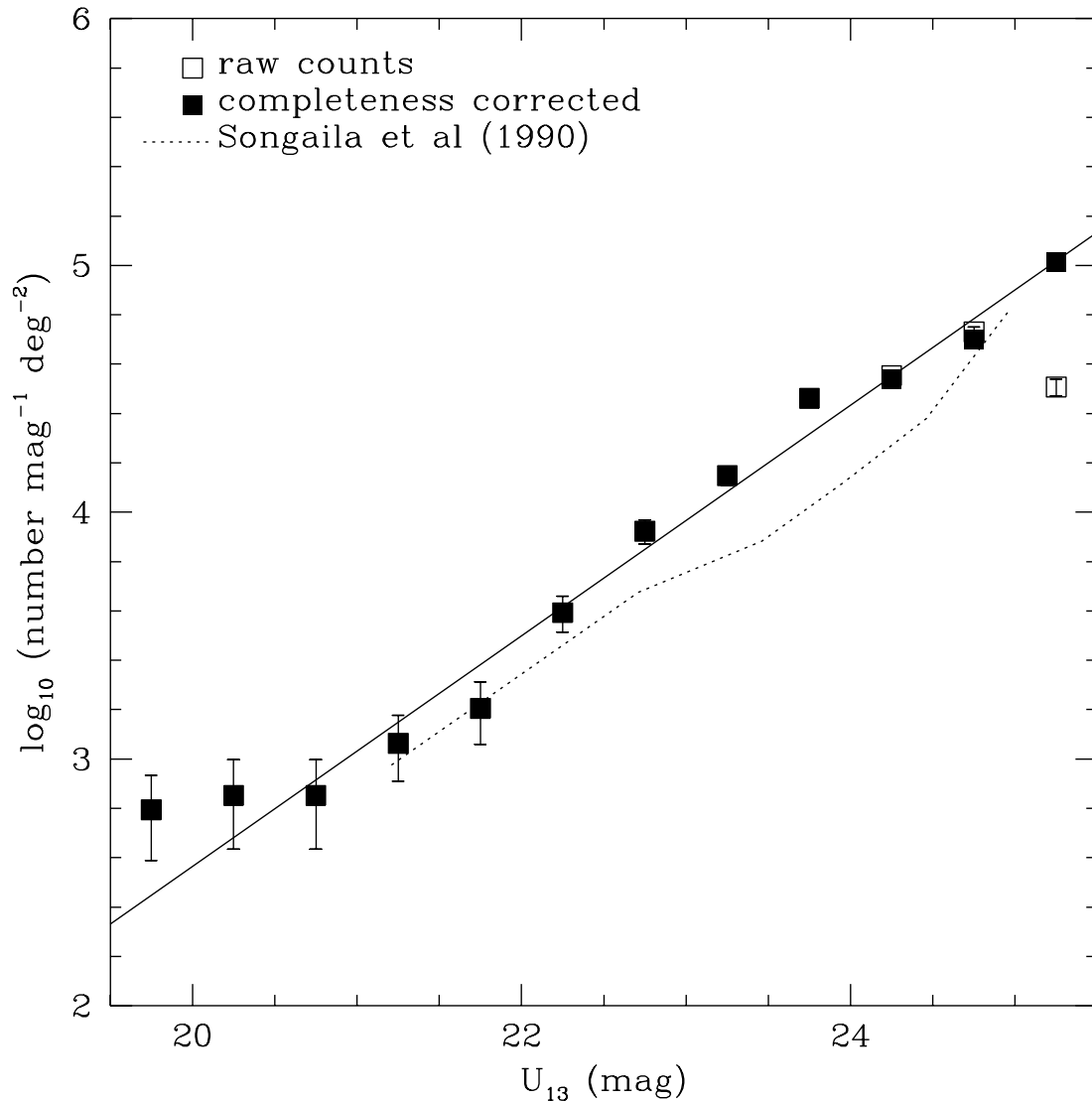
Fig. 3.— The U_{13}-band number counts. Open squares are the positive counts with the "noise" counts (negative counts, see text) subtracted, from the data presented here; error bars are Poisson noise for the difference. Filled squares are the completeness-corrected counts (see text), also from the data presented here. The solid line is a fit to the corrected counts; it has slope $d\log N/dm = 0.467$. The dotted line shows counts of Songaila et al (1990), converted to this magnitude system assuming $U_{13} \approx U'_{AB} - 0.79$ mag for a typical object.
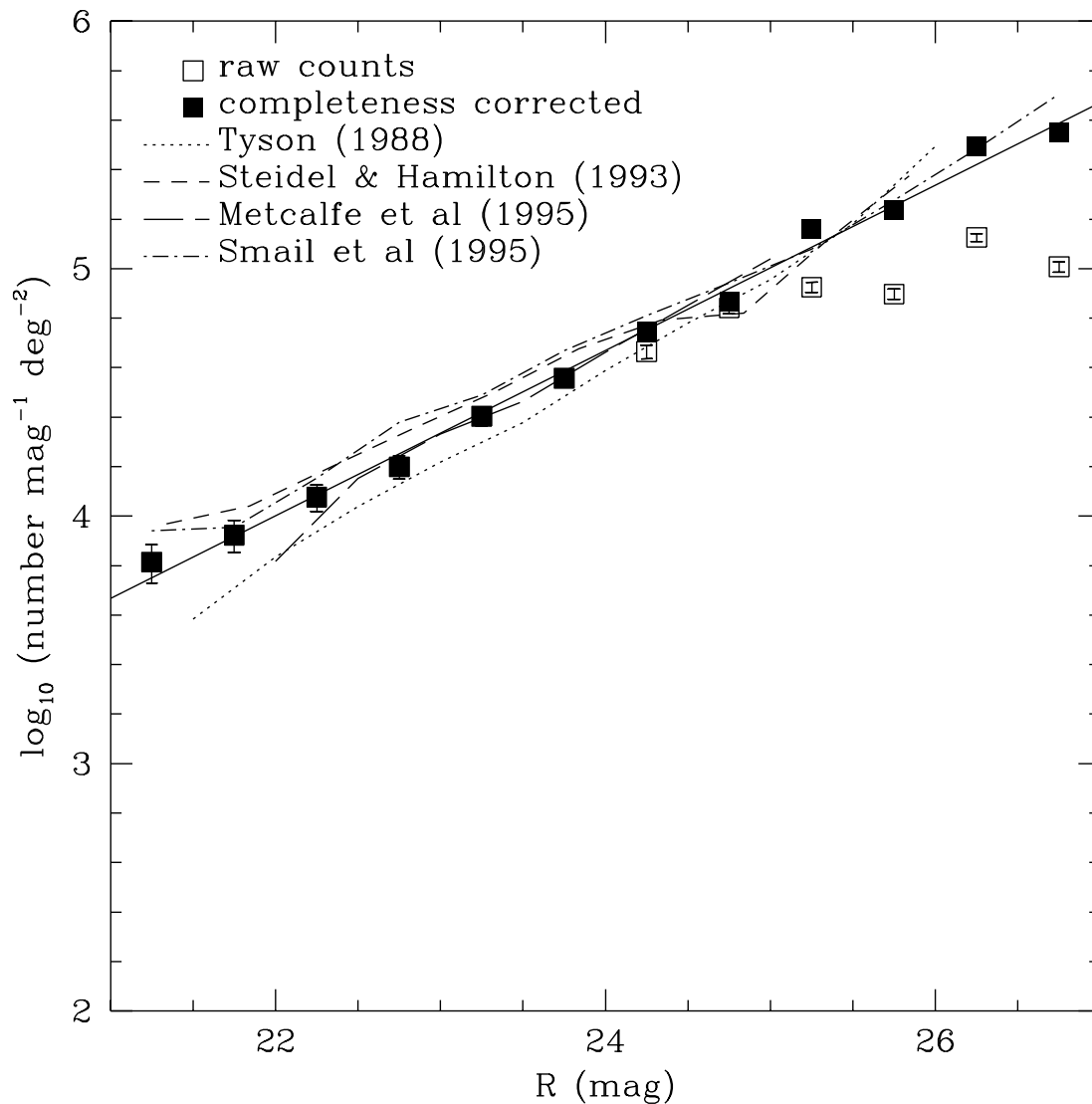
Fig. 4.— The R-band number counts. Open squares are the positive counts with the "noise" counts (negative counts, see text) subtracted, from the data presented here; error bars are Poisson noise for the difference. Filled squares are the completeness-corrected counts (see text), also from the data presented here. The solid line is a fit to the corrected counts; it has slope $d \log N/dm = 0.334$. Dashed and dotted lines are the completeness-corrected counts of other authors. The Steidel & Hamilton (1993) counts have been converted to this magnitude system assuming $R \approx \mathcal{R}_{AB} - 0.16$ for a typical object.
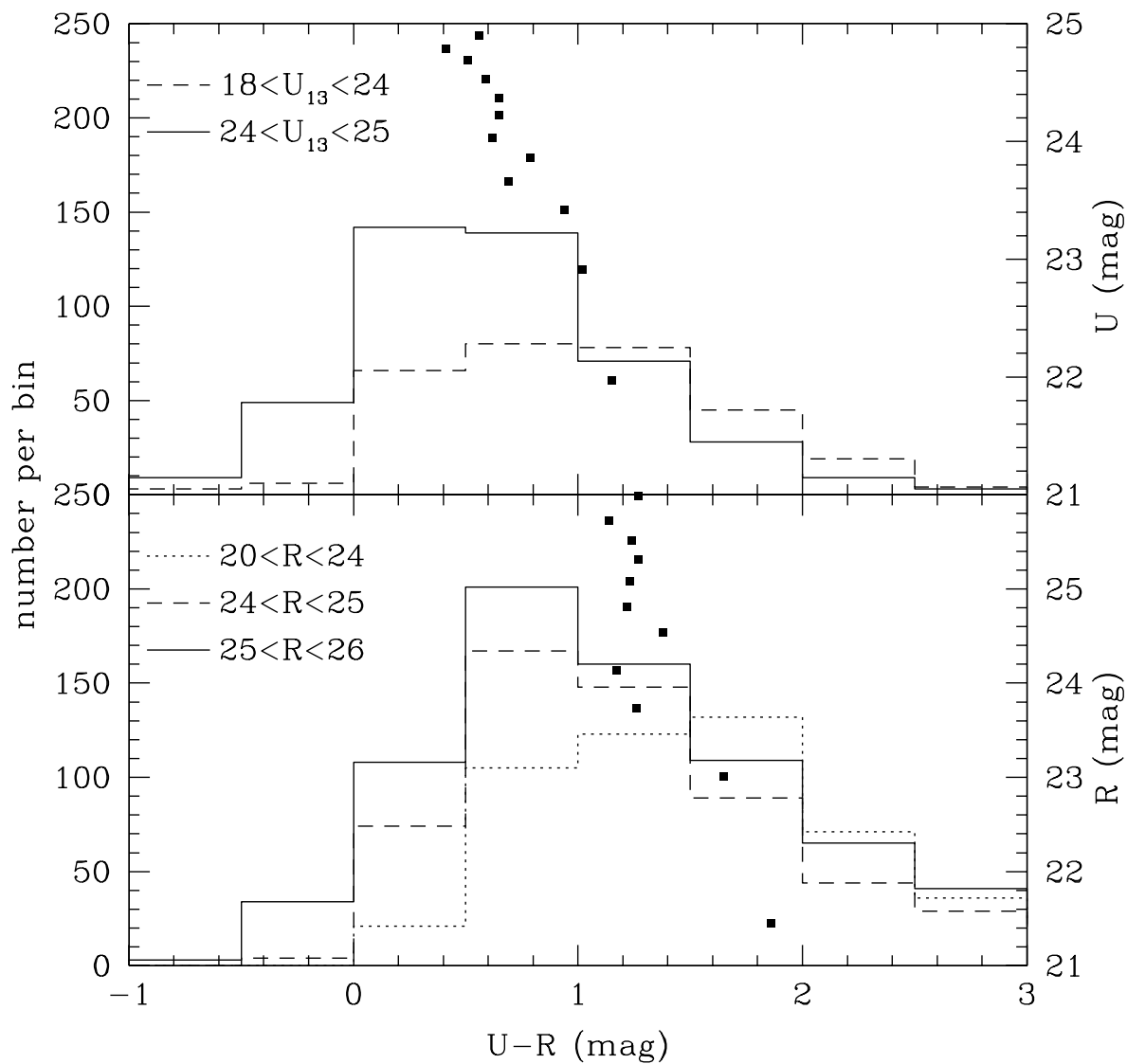
Fig. 5.— Histograms of $U - R$ colors (corrected to the standard U-band) through 1.5 arcsec apertures for several U-selected (top) and R-selected (bottom) samples. The squares show median colors as a function of magnitude, medianed in groups of 61 in the U-band and groups of 201 in the R-band.

R-band magnitude bin it is $U - R = 1.3$ mag, although clearly there are large magnitude uncertainties in the U-band data for such faint objects.

4. Results and discussion

4.1. Colors and faint-end count slopes

The faint ends of the counts have different slopes in the U and R bands, which means, under fairly robust assumptions, the mean object color must be a strong function of magnitude, a trend clearly visible in the color-magnitude diagram. Since the night sky would be infinitely bright in the U band if this trend continued forever, at some faint magnitude the U-band count slope must break to match the R-band slope and thereby end the bluing trend. One physical explanation for the bluing trend is that the fraction of the radiation due to young stars may increase with apparent magnitude. In this scenario, the objects should get no bluer than about $f_\nu \propto \nu^0$, the ultraviolet spectral slope of a star-forming galaxy (Kinney et al 1993), so a natural prediction is that the break in the U-band counts will appear when the median $(U - R)$ obtains the $f_\nu \propto \nu^0$ value, -0.4 mag. This should happen at $27 < U < 28$ mag. Very deep counts in the Hubble Deep Field data (Williams et al 1996), which reach point-source detection levels several magnitudes fainter than these observations, report a break at $U \sim 25.3$, although it is not robustly detected.

As is shown in Figures 3 and 4, the U-band counts found here are in good agreement with the previous study near this depth (Songaila et al 1990), the R-band counts are also in very good agreement with previous studies (Smail et al 1995; Metcalfe et al 1995; Steidel & Hamilton 1993; Tyson 1988) as are the colors (Guhathakurta et al 1990; Steidel & Hamilton 1993). The results here are similar to those of Guhathakurta et al (1990) except that the latter have $< 2.7 \times 10^5$ sources per square degree and only identify sources to $R \approx 26$, although that limit is fuzzy because sources were identified by those authors not in a single band but in a summed UBR image.

4.2. The number problem

We count faint objects in the U and R-bands to surface densities, integrated over flux, of 1.2×10^5 per square degree to $U = 25.5$ mag and 6.3×10^5 per square degree to $R = 27$ mag. These numbers correspond to 0.5 and 2.5×10^{10} objects over the entire sky. These numbers are in excess of the total number of galaxies expected within the observable Universe in any no-evolution or passive-evolution model (i.e., models in which the comoving

number density of galaxies is conserved), for the following simple reason: If the local galaxy luminosity function is that given by Loveday et al (1992) (or Mobasher et al 1993; or Lin et al 1996) and galaxies exist down to luminosities 5 mag fainter than L^*, the space density of galaxies is $5.7 \times 10^{-2} h^3$ Mpc^{-3}, where h is the Hubble constant in units of 100 km s^{-1} Mpc^{-1}. In units of Hubble volume $V_H \equiv (c/H_0)^3$, this corresponds to a density of $1.5 \times 10^9 V_H^{-1}$. This number density increases by only $3.5 \times 10^8 V_H^{-1}$ per magnitude as the luminosity function is extrapolated at the faint end. In an Einstein-de Sitter universe, $(\Omega_M, \Omega_\Lambda) = (1, 0)$, there is an all-sky comoving volume of only $4.2 V_H$ to $z = 3$. The product of number density and volume is 6×10^9 galaxies of the entire sky, so there are 4 times too many sources observed in these data to be easily explained by naive models. The number of galaxies increases with apparent magnitude, so the problem is worse with deeper data: Cowie et al (1996) show a factor of 10 times too many sources, and the counts in the HDF (Williams et al 1996) show a factor of at least 15 times too many sources. We know that only a small fraction of the galaxies presented here lie beyond $z \approx 3$ because at this redshift the Lyman limit redshifts into the U-band and the flux is cut off by either self-absorption or absorption in intervening material (e.g., Guhathakurta et al 1990; Steidel et al 1995, 1996); 73 percent of the sources to $R = 27$ mag are detected in U_{13}. Of course these numbers are consistent with the population of galaxies at $z > 3$ found and confirmed spectroscopically by Steidel et al (1995; 1996), because that high redshift population is only a few percent of the total source counts.

For $(\Omega_M, \Omega_\Lambda) = (0.05, 0)$ the comoving volume is $14 V_H$, for $(\Omega_M, \Omega_\Lambda) = (0.2, 0.8)$ it is $19 V_H$, so switching world models does not solve the problem unless one considers even more extreme world models that are almost certainly ruled out by gravitational lens statistics (Turner 1990). Several authors have found local luminosity function amplitudes higher than that of Loveday et al (1992) by factors of a few (Marzke et al 1994; Lilly et al 1995; Small 1996) but factors large enough to solve the number problem would be surprising. There is also some disagreement over the faint-end slope α (in the parameterization $\phi(L) \propto L^\alpha$) of the local luminosity function (e.g., Lilly et al 1995). If the slope is steeper than the standard flat value (i.e., if α is more negative than $\alpha = -1.0$), there could be significantly more galaxies in the local Universe than the above estimates suggest. For example, comparing with $\alpha = -1.0$, if $\alpha = -1.5$ but L^* and the bright-end amplitude are held fixed, there is a factor of ≈ 5 more galaxies to a luminosity limit of 5 mag fainter than L^*. This would go some way towards alleviating the number problem, although the slope is well-enough determined by local surveys that such a large discrepancy seems unlikely.

With current observational constraints, it is more natural to look to evolution in the sources to solve the number problem. It has been suggested that the galaxy merging rate is high, so large numbers of small galaxies at high redshift evolve into small numbers of

large galaxies locally (Guiderdone & Rocca-Volmerange 1991; Broadhurst et al 1992). It is possible that there is a large population of small galaxies which explode or evaporate after their first burst of star formation and supernovae (Babul & Rees 1992). Also, there is a less-explored possibility that galaxies may form at high redshift with more-or-less their present-day masses but if star formation occurs in small, spatially isolated bursts (Katz 1992), each present-day galaxy would be observed as many different objects at large lookback time. There may be support for some of these models in the redshift distribution of faint galaxies; several authors have found a steepening of the faint-end slope of the luminosity function with redshift (Eales 1993; Lilly et al 1995; Ellis et al 1996), and enormous information will come from the current generation of super-deep redshift surveys (e.g. Cowie et al 1996; Cohen et al 1996a, 1996b; Koo et al 1996).

4.3. Stronger redshift limits with HST

The ultraviolet sensitivies of the WFPC2 and STIS instruments (the latter to be installed in 1997) on HST suggest the extension of this technique—limiting redshift distributions by looking for the Lyman limit break—to lower redshift. In fact, the broadband UV filters of these instruments can actually be used to locate the Lyman break over a range of redshifts from 0.9 to 1.8, a range which is difficult to identify at present even with 10-m–class telescopes because there are very few lines in the useful window of ground-based visual spectrocopy. With a modest amount of observing time it will be possible to obtain at least statistical redshift distributions significantly deeper than the practical limits of ground-based spectroscopy even if there were spectroscopic features in this redshift range. Such observations are particularly crucial since many of the above-mentioned models make very different predictions for the fraction of galaxies at $z > 1$ and $z > 2$.

REFERENCES

Babul A., Rees M. J., 1992, MNRAS, 255, 346

Bertin E., Arnouts S., 1996, A&AS, 117, 393

Broadhurst T. J., Ellis R. S., Glazebrook K., 1992, Nature, 355, 55

Burstein D., Heiles C., 1982, AJ, 87, 1165

Cohen J. G., Hogg D. W., Pahre M. A., Blandford R. D., 1996a, ApJ, 462, L9

Cohen J. G., Cowie L. L., Hogg D. W., Songaila A., Blandford R. D., Hu E. M. & Shopbell P., 1996b, ApJ, 471, L5

Cohen J. G. et al, 1996c, in preparation

Cowie L. L., Hu E. M., Songaila A., 1995, AJ, 110, 1576

Djorgovski S. et al, 1995, ApJ, 438, L13

Dressler A., 1993, in Neugebauer G., ed., *Palomar Observatory Annual Report 1993,* 2

Driver S. P., Windhorst R. A., Griffiths R. E., 1995, ApJ, 453, 48

Eales S., 1993, ApJ, 404, 51

Ellis R. S., Colless M. M., Broadhurst T. J., Heyl J. S., Glazebrook K., 1996, MNRAS, 280, 235

Griffiths R. E. et al., 1994, ApJ, 435, L19

Guhathakurta P., Tyson J. A., Majewski S. R., 1990, ApJ, 357, L9

Guiderdone B., Rocca-Volmerange B., 1991, A&A, 252, 435

Hall P., Mackay C. D., 1984, MNRAS, 210, 979

Im M., Casertano S., Griffiths R. E., Ratnatunga K. U. & Tyson J. A., 1995, ApJ, 441, 494

Jones L. R., Fong R., Shanks T., Ellis R. S., Peterson B. A., 1991, MNRAS, 249, 481

Katz N., 1992, ApJ, 391, 502

Kinney A. L., Bohlin R. C., Calzetti D., Panagia N., Wyse R. F. G., 1993, ApJS, 86, 5

Kochanek C. S., 1992, ApJ, 384, 1

Koo D. C., 1986, ApJ, 311, 651

Koo, D. C. & Kron, R. G., 1992, ARA&A, 30, 613

Koo D. C., Gronwall C., Bruzual G. A., 1993, ApJ, 415, L21

Koo D. C., et al, 1996, ApJ, 469, 535

Lilly S. J., Tresse L., Hammer F., Le Fevre O., Crampton D., 1995, ApJ, 455, 108

Lin H., Kirshner R. P., Shectman S. A., Landy S. D., Oemler A., Tucker D. L., Schechter P. L., 1996, ApJ, 464, 60

Loveday J., Peterson B. A., Efstathiou G., Maddox S. J., 1992, ApJ, 390, 338

Marzke R. O., Huchra J. P., Geller M. J., 1994, AJ, 108, 437

Metcalfe N., Shanks T., Fong R., Roche N., 1995, MNRAS, 273, 257

Mobasher B., Sharples R. M., Ellis R. S., 1993, MNRAS, 263, 560

Oke J.B. et al., 1995, PASP 107, 375

Pahre M. A. et al, 1996, in preparation

Smail I., Hogg D. W., Yan L., Cohen J. G., 1995, ApJ, 449, L105

Small T. A., 1996, PhD thesis, California Institute of Technology

Songaila A., Cowie L. L., Lilly S. J., 1990, ApJ, 348, 371

Steidel C. C., Hamilton D., 1993, AJ, 105, 2017

Steidel C. C., Pettini M., Hamilton D., 1995, AJ, 110, 2017

Steidel C. C., Giavalisco M., Pettini M., Dickinson M., Adelberger K., 1996, ApJ, 462, L17

Turner E. L., 1990, ApJ, 365, L43

Tyson J. A., 1988, AJ, 96, 1

Williams R. et al., 1996, AJ, 112, 1335

Table 1.   Imaging data

band	instrument	field area (arcmin^2)	total $t_{\exp}$ (s)	pixel scale (arcsec)	seeing[a] (arcsec)	$3\,\sigma$ detection[b] (mag)
U_{13}	Hale/COSMIC/CCD13	81	28000	0.28	1.1	26.36
U	P60/CCD13	160	5400	0.37	2.2	23.13
R	Keck/LRIS	39	8400	0.22	0.8	28.01
R_{C}	P60/CCD13	160	600	0.37	1.3	23.25

[a] Seeing FWHM in final, stacked images

[b] Signal-to-noise ratio of 3 through an aperture of diameter 1.5 times the seeing FWHM, with no aperture correction applied